



Contents lists available at ScienceDirect

Journal of King Saud University – Science

journal homepage: www.sciencedirect.com

Review

Structural, dielectric and electrical properties of new Ni-doped copper/bentonite composite

M.G. Althobaiti^a, Marwa Belhaj^{b,c}, T. Abdel-Baset^{c,d}, Ali H. Bashal^e, Abdullah A. Alotaibi^{f,*}^a Department of Physics, College of Science, Taif University, P.O.Box 11099, Taif 21944, Saudi Arabia^b NANOMISENE Laboratory LR16CRMN01, Center of Research in Microelectronic and Nanotechnology of Sousse, Technopark of Sousse, BP 334, 4050 Sousse, Tunisia^c Department of Physics, Faculty of Science, Taibah University, Yanbu 46423, Saudi Arabia^d Physics Department, Fayoum University, Fayoum 63514, Egypt^e Department of Chemistry, College of Science, Yanbu-30799, Taibah University, Al-Madina, Saudi Arabia^f Department of Chemistry, College of Science and Humanities, Shaqra University, 11911 Ad-Dawadmi, Saudi Arabia

ARTICLE INFO

Article history:

Received 10 March 2022

Revised 4 May 2022

Accepted 24 May 2022

Available online 28 May 2022

Keywords:

Ni/Cu-bentonite composite

Wet impregnation process

Dielectric properties

Conductivity

ABSTRACT

This paper describes the synthesis and characterization of pure bentonite as well as nanocomposites with varying ratios of nickel (Ni) and metallic copper (Cu) based on the wet impregnation method. Both XRD (X-ray diffraction) and SEM-EDX (scanning electron microscopy with energy-dispersive X-ray spectroscopy) analyses confirm the structural characteristics of the composites. The emergence of a Ni peak in the Cu/bentonite EDX spectra indicates that it is in the proper spot and is most likely the creation of Ni–Cu oxides. Furthermore, the dielectric characteristics and electrical conductivity of Ni-loaded Cu/bentonite composites were also measured at temperatures ranging from 25 °C to 120 °C and at a frequency range of 100 Hz–0.3 MHz to investigate the impact of varying Ni ratios. For all nanocomposite samples, the dielectric constant (ϵ') was shown to decrease with increasing frequency and rise with increasing Ni content. The dielectric modulus M'' resulted in a significant decrease in relaxation time. The associated barrier hopping conduction process was discovered to boost electric conductivity σ_{ac} at higher frequencies (CBH).

© 2022 The Author(s). Published by Elsevier B.V. on behalf of King Saud University. This is an open access article under the CC BY license (<http://creativecommons.org/licenses/by/4.0/>).

Contents

1. Introduction	2
2. Experimental methods and procedures	2
2.1. Reagents	2
2.2. Synthesis of the composites	2
2.3. Characterization of composites	3
3. Results and discussion	3
3.1. XRD analysis	3
3.2. SEM/EDX analysis	4
3.3. Dielectric analysis	5
3.3.1. Dielectric properties	5
3.3.2. Ac conductivity (σ_{ac})	5
4. Conclusion	5

* Corresponding author.

E-mail address: aaalotaibi@su.edu.sa (A.A. Alotaibi).

Peer review under responsibility of King Saud University.



Production and hosting by Elsevier

<https://doi.org/10.1016/j.jksus.2022.102127>

1018-3647/© 2022 The Author(s). Published by Elsevier B.V. on behalf of King Saud University.

This is an open access article under the CC BY license (<http://creativecommons.org/licenses/by/4.0/>).

Declaration of Competing Interest	5
Acknowledgements	5
References	5

1. Introduction

Recently, a wide scientific interest has been in environmental aspects of research and industrial fields. One of the most important of these interests is the methods of storing clean energy alternatives such as storing electricity and its conversion into different energy forms to meet the demands and needs of consumers. Electrochemical supercapacitors, defined as a type of microelectronic component, can be charged/discharged as a storing main of energy and possible use of that stored energy for long periods (Conway and Pell, 2003). It is noted that much scientific research focuses on the development, optimizing, and manufacturing of capacitor-with increased efficiency in energy storage (Deng et al., 2011). Bentonite is one of the clay minerals that can be classified into the smectite group. Moreover, Bentonite is mainly composed of montmorillonite and hydrated aluminum silicate (Saltas et al., 2008). The composition of bentonite consists mainly of 70 % silicon oxide with a small portion of aluminum oxide estimated at 15 % (Jiang et al., 2008). In general, the chemical formula can be written in the form $Nax(H_2O)_4(Al_{2-x}Mg_{0.83})Si_4O_{10}(OH)_2$ (Sang et al., 2007).

The crystal structure of montmorillonite consists of two layers of two tetrahedral sheets of SiO_4 compound with an octahedral sheet of the $Al(O, OH)_6$ compound sandwiched between them (Saltas et al., 2008). A layered-structure Bentonite with large amounts of medium pores readily available has low-cost, widely spread, and environmentally friendly (Jeenpadiphat and Tungasmita, 2014). Because Bentonite shows a strong coherence-between metal and support, it can be used as catalytic support and it has various applications in the field of catalysis (Li et al., 2020; Amaya et al., 2020). Bentonite has good adsorption efficiency of heavy metal ions for industrial wastewater treatment (Kakaei et al., 2020). In addition, it is used as inorganic fillers needed to prepare alkaline polymer compounds with high conductivity.

Many studies have been done to verify the electrical conductivity of bentonite. Sang et al. reported that bentonite has contradictory effects (positive and negative) on the ionic conductivity of the solid alkaline polymer electrolyte (Sallam et al., 2017). However, studying the electrical conductivity of powders and porous materials is relatively complex. For a decade, many research studies have focused on the development of a range of transition metal oxides for use as electrode-active materials for electrochemical capacitors (ECs). Transition metal oxides can be classified as oxides of noble or base metals such as MnO_2 and NiO (Conway and Pell, 2003). Because of the pseudo-capacitive behavior, the low-cost value, and the environmental friendliness, these materials might be considered compared to RuO_2 which is a modern supercapacitor material (Conway and Pell, 2003). In the case of a solid substance, the crystal structure of nickel is in the form of a face-centered cube (fcc). The electrical resistivity of nickel is $48.66 n\Omega \cdot m$ at $20^\circ C$. Nickel has many uses and applications, for example, nickel participate in the manufacture of metal alloys, batteries, coins, etc (Karimzadeh et al., 2019; Gombac et al., 2010). Copper (Cu) is considered as the appropriate dopant for many metal oxides such as TiO_2 in several applications. Copper oxides (CuO and Cu_2O) have photocatalytic activity similar to that of the noble metals, bandgap value of 1.4 and 2.2 eV respectively, a negative value of the conduction bands moderator, which is estimated at (-0.96 and -0.22 V), and high value of the light absorption coefficient (Tantawy et al., 2021; El-Maghrabi et al., 2021; El-Maghrabi et al., 2020; Kawrani et al., 2020; Buchholz et al., 2005).

Buchhok et al. were able to successfully manufacture a low-concentration magnetic semiconductor with copper-doped ZnO (Wu et al., 2007). In addition, Wu et al. produced AlN doped with copper, which contributed to narrowing the ferromagnetic band-gap, increasing the long-wave absorption value, and contributing to reducing the energy loss value significantly after doping (Wang et al., 2015). Wang et al. investigated the nanostructure of ZnO saturated with copper and delineated the magnetic properties of copper (Bashal et al., 2020).

In the present study, 5 % Cu/bentonite composites have synthesized with 1 %, 3 %, and 5 % loadings of Ni by wet impregnation method. The effects of Ni doping on the structure, morphology of the surface, dielectric and electrical properties of Cu/bentonite are probed and quantified.

2. Experimental methods and procedures

2.1. Reagents

Bentonite and copper (II) chloride ($CuCl_2$) the product of Sigma-Aldrich were bought. Nickel (II) chloride product of Asagga-Pharma-HOLYLAND, Kingdom of Saudi Arabia was obtained. Deionized water (DI) was used in preparing all aqueous solutions. The Ni and Cu-based bentonite composites were synthesized following the incipient wet impregnation method. All chemicals and reagents were used as received without further refinement.

2.2. Synthesis of the composites

Monometallic and bimetallic bentonite nanocomposites were synthesized using the incipient wet impregnation method as described in (Kıpçak and Kalpazan, 2020). For monometallic composite, pure bentonite was dispersed in water under vigorous stirring for 30 min. Then, the 5 wt% $CuCl_2$ solution prepared in 3 mL of DI, were dropped into the stirred bentonite solution. Then the final mixture was left for 12 h at room temperature. After finishing the reaction the obtained nanocomposite was dried overnight at $120^\circ C$. For bimetallic nanocomposites, the solution of $CuCl_2$ and $NiCl_2$ was prepared in 6 mL of DI. The mixed solution of Cu/Ni was dropped into the dispersed bentonite solution and stirred for

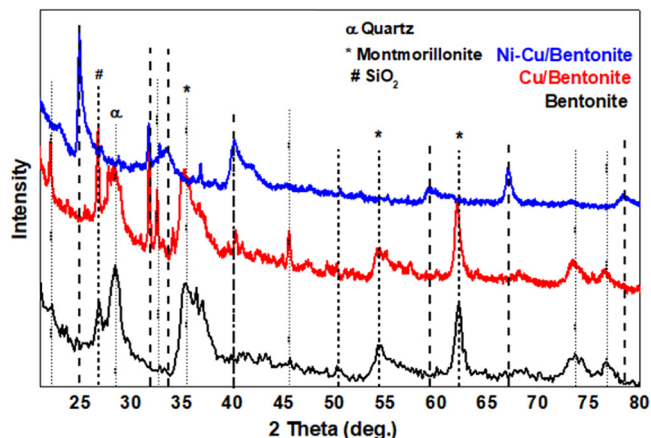


Fig. 1. The XRD patterns of pure bentonite and composites (Cu/bentonite, and Ni-Cu/bentonite).

12 h. Then, the solution was left in the oven to dry overnight. The 5 wt% Cu loaded composite was marked as 5 % Cu/bentonite. While in the case of bimetallic composite, 5 % Ni was doped with 5 % Cu and the obtained composite was marked as 5 %Ni-5 %Cu/bentonite. Cu and Ni-supported bentonite composites predominantly had a solid white appearance.

2.3. Characterization of composites

X-ray diffractometer (JEOL JDX-8030, Tokyo, Japan) with monochromated Cu-K α radiation of wavelength (λ) 1.5418 Å within the 2θ range of 20°–70° was used to confirm the existence of the incorporated ingredients. The morphology of the prepared nanocomposites was scanned by JEOL JSM-IT300, Tokyo, Japan SEM instrument. In addition, the analysis of surface elements was accomplished using the EDX (Oxford, UK) peripheral equipped with the SEM instrument.

The dielectric properties of the synthesized nanocomposite-spread in circular pellets (~1 mm thick and ~ 0.5 cm in radius) were recorded using Solartron frequency and analytical response analyzer. The sample pellets were attached to the resistor (47 Ω)

to stabilize the signal. The findings were recorded in the frequency range of 0.1 kHz to 0.3 MHz at room temperature.

3. Results and discussion

3.1. XRD analysis

Fig. 1 shows the XRD patterns of pure bentonite, Cu/bentonite, and Ni-Cu/bentonite synthesized via the incipient wet impregnation process. The pattern of pure bentonite confirms the dominance of montmorillonite mineral (peaks marked by *) as the main bentonite component with diffraction peaks at $2\theta = 19.8^\circ$, 35.2° , and 54.7° corresponding to the (101), (107) and (144) planes of montmorillonite. This pattern confirmed that the support is typical bentonite (Srinivasan and Punithavelan, 2018). Other peaks corresponding to the impurities like quartz and SiO₂ are also distinguishable at $2\theta = 22.2^\circ$, 26.8° , and 36.4° . XRD patterns of the Cu/bentonite sample show the characteristic reflections at $2\theta = 16.20^\circ$, 21.99° , 32.52° , 40.25° and 45.52° ascribed to the (110), (020), (201), (221) and (311) planes of CuCl₂·2H₂O, respectively. Apart from the above-mentioned peaks, others at $2\theta = 37.2^\circ$, 43.3° and

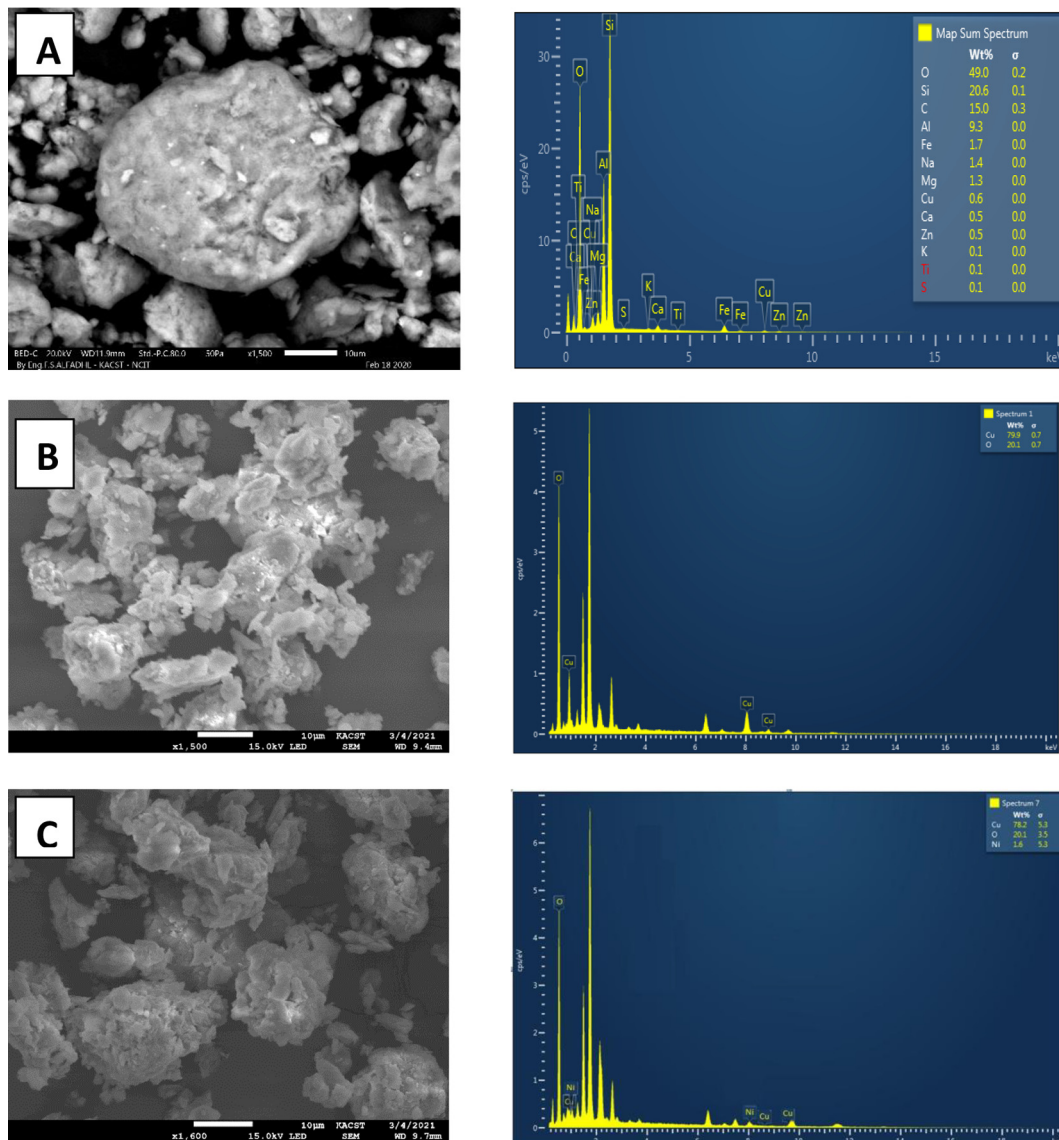


Fig. 2. SEM-micrographs and EDX spectra for (A) pure bentonite, (B) Cu/bentonite, (C) Ni-Cu/bentonite.

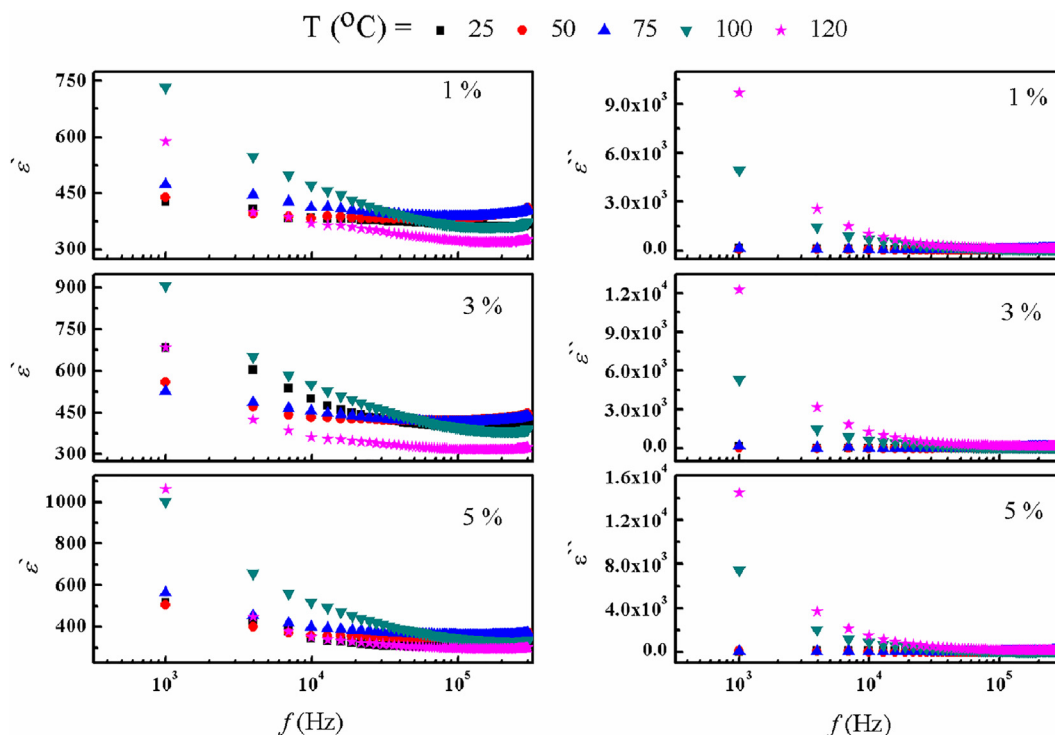


Fig. 3. ϵ' and ϵ'' as a function of temperature for 1%, 3% and 5% Ni doped (5% Cu - bento).

79.14° were detected in Ni-Cu/bentonite that ascertained to the planes (111), (200), and (222) of the NiO cubic phase (JCPDS card NO. 47-1049), respectively. Moreover, the intensity of Cu diffraction peaks in the Ni-Cu/bentonite was weakened remarkably compared to that in the Cu/bentonite and shifted to higher angles due to the intervention between Cu, Ni, and bentonite.

3.2. SEM/EDX analysis

Fig. 2(A, B and C) shows the surface morphology of bentonite, Cu/ bentonite, and Cu-Ni/bentonite, respectively. As can be seen, bentonite (Fig. 2A) exhibits a microstructure with different particle sizes and a slightly rough and porous surface morphology. In Fig. 2B, the Cu/bentonite morphology shows a flaky structure and a relatively rougher surface compared to that of pure bentonite which can be imputed to the large surface area of bentonite that allows more ions adsorption. As for Cu-Ni/bentonite microstruc-

Table 1

The relaxation time and the activation energy for 1%, 3% and 5% Ni doped 5% Cu - bentonite.

Ni contents	τ (μ s)	E_a (eV)
1 %	4.03	0.432
3 %	3.29	0.439
5 %	2.78	0.444

ture, it reveals a higher number of aggregated clusters indicating greater adsorption in the inner surface.

The elemental analyses of pure bentonite, Cu/bentonite, Ni-Cu/ bentonite composites are presented in Fig. 2. The results confirm the presence of the expected elements forming bentonite, i.e., silicon (Si) and aluminum (Al) in addition to minor amounts of iron (Fe), magnesium (Mg), calcium (Ca), and potassium (K). The bentonite-based composites spectra present a good agreement between the elemental compositions and the that used for preparing

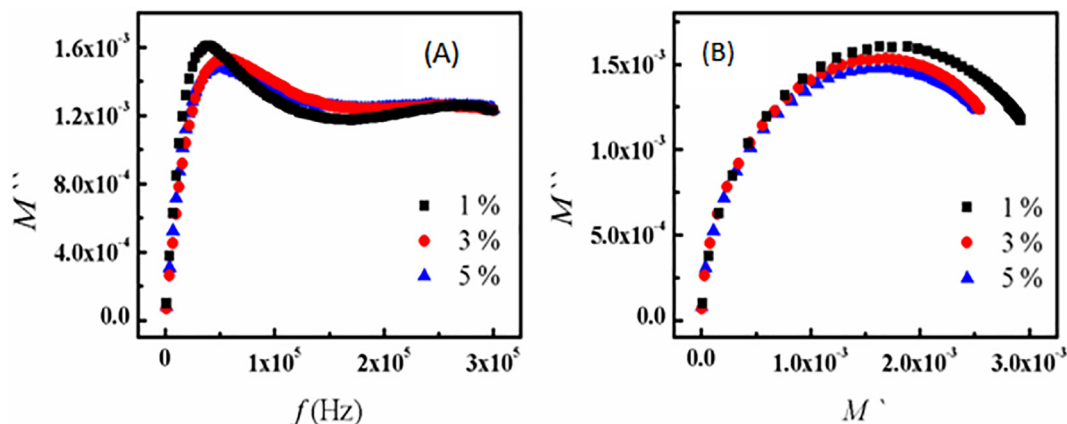


Fig. 4. (A) Frequency dependence of M'' and (B) M' versus M'' for 1%, 3% and 5% Ni doped (5% Cu - bento) at 120 °C, respectively.

each composite. This trend confirms the incorporation of Cu and Ni in the bentonite matrix (bentonite-Cu and bentonite-Cu-Ni).

3.3. Dielectric analysis

3.3.1. Dielectric properties

Charting dielectric constant (ϵ') and dielectric loss (ϵ'') versus frequency at different temperatures for 1 %, 3 %, and 5 % Ni-doped 5 % Cu / bentonite respectively are shown in Fig. 3. ϵ' and ϵ'' are found to be in inverse proportional to frequency, which maybe attributed to domain walls reductions, and the ease orientation of more dipoles to the applied field direction. Moreover, the values of ϵ' and ϵ'' increase with increasing Ni concentration which maybe attributed to Maxwell–Wagner and space-charge polarization (Abdel-Baset and Bashal, 2020). Finally, it was observed that the ϵ' values increase with increasing temperature for all prepared samples.

Fig. 4(A) shows the frequency dependence of the imaginary part of the electric modulus M'' at 120 °C for 1 %, 3 %, and 5 % Ni-doped 5 % Cu-bentonite. As shown, the peak strength (M''_{\max}) increases with increasing Ni concentration, whereas the peak frequency becomes lower with increasing Ni content, which is related to Maxwell Wegner polarization. The relaxation time of the samples was calculated from the inverse of the angular frequency of M'' maximum ($\tau = 1/2\pi f_{\max}$). The values of τ are listed in Table 1, and they have been used to calculate the values of the activation energy E_a following the equation:

$$E_a = \tau_0 e^{-E_a/kT}$$

Data of Table 1, shows that the relaxation time increases while the activation energy decreases with increasing Ni concentration. The relation between M'' and M' (Cole-Cole plot) at 120 °C is shown in Fig. 4(B). The results indicate semi-circles with diameter that increase with decreasing Ni content confirming the reduction of impedance and relaxation time and thus increasing connectivity.

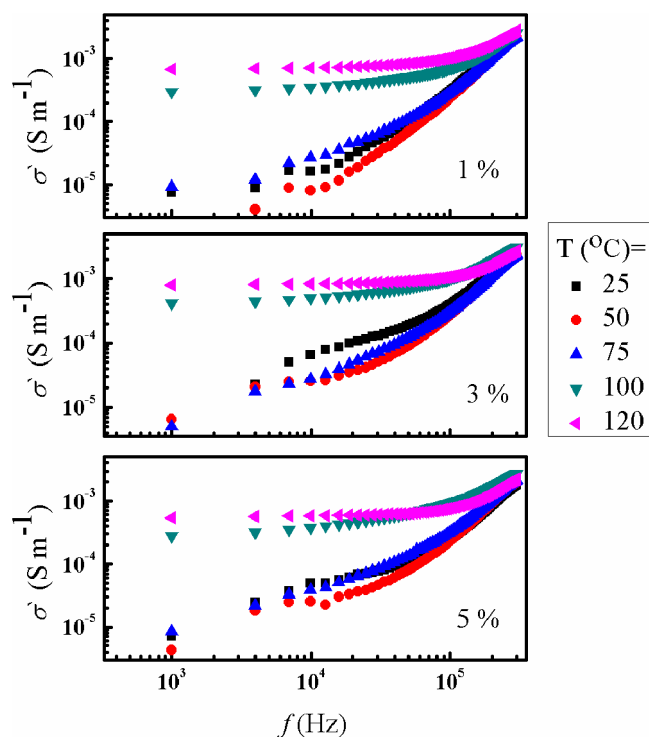


Fig. 5. Dependence of σ_{ac} on Frequency at fixed temperature for 1%, 3%, and 5% Ni doped 5% Cu –bentonite.

3.3.2. Ac conductivity (σ_{ac})

The ac conductivity (σ_{ac}) value as a function of frequency calculated using the following equation (Abou Elfadl et al., 2020):

$$\sigma_{ac} = \sigma_t - \sigma_{dc} = \omega \epsilon_0 \epsilon' \tan \delta \quad (1)$$

where; σ_t : total conductivity, σ_{dc} : low-frequency conductivity, ω : angular frequency, ϵ_0 : permittivity of the free space, and $\tan \delta$: loss tangent. Dependence of σ_{ac} on frequency for 1 %, 3 %, and 5 % Ni-doped 5 % Cu/ bentonite, at different fixed temperatures is depicted in Fig. 5. The electrical conductivity values are nearly constant at low frequencies, which maybe ascertained to the dc conductivity. On contrary, by increasing frequency, the conductivity ramps slightly indicating the transport of the charge carriers by hopping via the defective sites along the chains. This attitude is a result of an increasing number of the charge carriers due to the increase of the absorbed energy which contributes to the conduction process [25].

4. Conclusion

Cu-Bentonite composites were effectively produced using the incipient wet impregnation procedure, as shown by XRD and EDX studies. The dielectric characteristics of Ni-Cu-bentonite composites were examined as a function of temperature and frequency. The dielectric constant and dielectric loss values were found to decrease with increasing frequency and vice versa with increasing Ni-content. The activation energy E_a values in the Cu-bentonite composite were observed to rise with increasing Ni content. In addition, the ac conductivity increased with increasing frequency, which might be the result of a hopping conduction mechanism. The strong dielectric characteristics and low activation energy for additional Ni in Cu-bentonite demonstrate its importance in dielectric applications.

Declaration of Competing Interest

The authors declare that they have no known competing financial interests or personal relationships that could have appeared to influence the work reported in this paper.

Acknowledgements

- The Authors thank Taif University Researchers Supporting Project number (TURSP-2020/272) Taif University, Taif, Saudi Arabia.
- The author would like to thank the Deanship of Scientific Research at Shaqra University for supporting this work.

References

- Abdel-Baset, T.A., Bashal, A.H., 2020. Structure and AC conductivity of zinc and nickel-doped TiO₂ nanocomposite synthesized by simple incipient wet impregnation method. *J. Mater. Sci. - Mater. Electron.* 31, 18533–18540. <https://doi.org/10.1007/s10854-020-04397-1>.
- Abou Elfadl, A., Is, A.M., Mohammed, M.I., 2020. Dielectric study and AC conduction mechanism of gamma irradiated nano-composite of polyvinyl alcohol matrix with Cd_{0.9}Mn_{0.1}S. *J. Mater. Sci. - Mater. Electron.* 31 (11), 8297–8307.
- Amaya, J., Suarez, N., Moreno, A., Moreno, S., Molina, R., 2020. Mo or W catalysts promoted with Ni or Co supported on modified bentonite for decanehydroconversion. *New J. Chem.* 44, 2966–2979. <https://doi.org/10.1039/C9NJ04878B>.
- Bashal, A.H., Saad, M.H., Khalafalla, M.A., 2020. The effect of nickel percentage on the dielectric properties of bentonite. *J. Taibah. Univ. Sci.* 14, 496–499. <https://doi.org/10.1080/16583655.2020.1747216>.
- Buchholz, D.B., Chang, R.P.H., Song, J.-Y., Ketterson, J.B., 2005. Room-temperature ferromagnetism in Cu-doped ZnO thin films. *Appl. Phys.* 87 (8), 082504.
- Conway, B.E., Pell, W.G., 2003. Double-layer and pseudocapacitance types of electrochemical capacitors and their applications to the development of hybrid devices. *J. Solid State Electrochem.* 7, 637–644. <https://doi.org/10.1007/s10008-003-0395-7>.

- Deng, W., Ji, X., Chen, Q., Banks, C.E., 2011. Electrochemical capacitors utilizing transition metal oxides: an update of recent developments. *RSC Adv.* 1, 1171–1178. <https://doi.org/10.1039/C1RA00664A>.
- El-Maghrabi, H.H., Nada, A.A., Roualdes, S., Bekheet, M.F., 2020. Design of Ni/NiO-TiO₂/rGO nanocomposites on carbon cloth conductors via PECVD for electrocatalytic water splitting. *Int. J. Hydrog. Energy* 45 (56), 32000–32011. <https://doi.org/10.1016/j.ijhydene.2020.08.259>.
- El-Maghrabi, H.H., Nada, A.A., Bekheet, M.F., Roualdes, S., Riedel, W., Iatsunskyi, I., Coy, E., Gurlo, A., Bechelany, M., 2021. Coaxial nanofibers of nickel/gadolinium oxide/nickel oxide as highly effective electrocatalysts for hydrogen evolution reaction. *J. Colloid Interface Sci.* 587, 457–466. <https://doi.org/10.1016/j.jcis.2020.11.103>.
- Gombac, V., Sordelli, L., Montini, T., Delgado, J.J., Adamski, A., Adami, G., Cargnello, M., Bernal, S., Fornasiero, P., 2010. CuO_x-TiO₂ photocatalysts for H₂ production from ethanol and glycerol solutions. *J. Phys. Chem. A* 114, 3916–3925. <https://doi.org/10.1021/jp907242q>.
- Jeenpadiphat, S., Tungasmita, D.N., 2014. Esterification of oleic acid and high acid content palm oil over an acid-activated bentonite catalyst. *Appl. Clay Sci.* 87, 272–277. <https://doi.org/10.1016/j.clay.2013.11.025>.
- Jiang, Y.X., Xu, H.J., Liang, D.W., Tong, Z.F., 2008. Adsorption of Basic Violet 14 from aqueous solution on bentonite. *C. R. Chim.* 11, 125–129. <https://doi.org/10.1016/j.crci.2007.04.005>.
- Kakaei, S., Khameneh, E.S., Rezazadeh, F., Hosseini, M.H., 2020. Heavy metal removing by modified bentonite and study of catalytic activity. *J. Mol. Struct.* 1199. <https://doi.org/10.1016/j.molstruc.2019.126989>. 126989.
- Karimzadeh, A., Aliofkhaezai, M., Wals, F.C., 2019. A review of electrodeposited Ni-Co alloy and composite coatings: Microstructure, properties and applications. *Surf. Coat. Technol.* 372, 463–498. <https://doi.org/10.1016/j.surfcoat.2019.04.079>.
- Kawrani, S., Boulos, M., Bekheet, M.F., Viter, R., Nada, A.A., Riedel, W., Roualdes, S., Cornu, D., Bechelany, M., 2020. Segregation of copper oxide on calcium copper titanate surface induced by Graphene Oxide for Water splitting applications. *Appl. Surf. Sci.* 516. <https://doi.org/10.1016/j.apsusc.2020.146051> 146051.
- Kıpçak, İ., Kalpazan, E., 2020. Preparation of CoB catalysts supported on raw and Na-exchanged bentonite clays and their application in hydrogen generation from the hydrolysis of NaBH₄. *Int. J. Hydrog. Energy* 45, 26434–26444. <https://doi.org/10.1016/j.ijhydene.2020.03.230>.
- Li, Z., Sun, Y., Yang, Y., Han, Y., Wang, T., Chen, J., Tsang, D.C., 2020. Comparing biochar-and bentonite-supported Fe-based catalysts for selective degradation of antibiotics: mechanisms and pathway. *Environ. Res.* 183. <https://doi.org/10.1016/j.envres.2020.109156>.
- Sallam, S.M., El-Saharty, A., Ahmed, A., 2017. Adsorption of toxic Ni (II) from an aqueous solution by bentonite. *Int. J. Ecotoxicol. Ecobiol.* 2, 158–165. <https://doi.org/10.11648/j.ijee.20170204.14>.
- Saltas, V., Vallianatos, F., Triantis, D., 2008. Dielectric properties of non-swelling bentonite: The effect of temperature and water saturation. *J. Non-Cryst. Solids* 354, 5533–5541. <https://doi.org/10.1016/j.jnoncrysol.2008.03.050>.
- Sang, S., Zhang, J., Wu, Q., Liao, Y., 2007. Influences of Bentonite on conductivity of composite solid alkaline polymer electrolyte PVA-Bentonite-KOH-H₂O. *Electrochim. Acta* 52, 7315–7321. <https://doi.org/10.1016/j.electacta.2007.06.004>.
- Srinivasan, M.P., Punithavelan, N., 2018. Structural, morphological and dielectric investigations on NiO/CuO/ZnO combined semiconductor metal oxide structures based ternary nanocomposites. *Mater. Res. Express.* 5. <https://doi.org/10.1088/2053-1591/aad079>. 075033.
- Tantawy, H.R., Nada, A.A., Baraka, A., Elsayed, M.A., 2021. Novel synthesis of bimetallic Ag-Cu nanocatalysts for rapid oxidative and reductive degradation of anionic and cationic dyes. *Appl. Surf. Sci.* 3. <https://doi.org/10.1016/j.apsadv.2021.100056> 100056.
- Wang, S.F., Chen, L.Y., Zhang, T., Song, Y.L., 2015. Half-metallic ferromagnetism in Cu-doped ZnO nanostructures from first-principle prediction. *J. Supercond. Nov. Magn.* 28, 2033–2038. <https://doi.org/10.1007/s10948-015-2964-2>.
- Wu, Q.Y., Huang, Z.G., Wu, R., Chen, L.J., 2007. Cu-doped AlN: a dilute magnetic semiconductor free of magnetic cations from first-principles study. *J. Phys.: Condens.* 19 (5), 056209.